Cell

Identification and Specification of the Mouse Skeletal Stem Cell

Charles K.F. Chan,[1,4,6,*] Eun Young Seo,[1,4,6] James Y. Chen,[2,6] David Lo,[1,4,6] Adrian McArdle,[1,4] Rahul Sinha,[2,4] Ruth Tevlin,[1,4] Jun Seita,[2,4] Justin Vincent-Tompkins,[2] Taylor Wearda,[1,4] Wan-Jin Lu,[2,4] Kshemendra Senarath-Yapa,[1] Michael T. Chung,[1] Owen Marecic,[1] Misha Tran,[1] Kelley S. Yan,[3] Rosalynd Upton,[2] Graham G. Walmsley,[1,4] Andrew S. Lee,[2] Debashis Sahoo,[2,4,5] Calvin J. Kuo,[3] Irving L. Weissman,[2,4,7] and Michael T. Longaker[1,4,7,*]

[1]Department of Surgery

[2]Departments of Pathology and Developmental Biology

[3]Stanford Cancer Institute

[4]Institute for Stem Cell Biology and Regenerative Medicine

Stanford University, 450 Serra Mall, Palo Alto, CA 94305, USA

[5]Department of Pediatrics, University of California, San Diego, 9500 Gilman Drive, La Jolla, CA 92093, USA

[6]Co-first author

[7]Co-senior author

*Correspondence: chazchan@stanford.edu (C.K.F.C.), longaker@stanford.edu (M.T.L.)

http://dx.doi.org/10.1016/j.cell.2014.12.002

SUMMARY

How are skeletal tissues derived from skeletal stem cells? Here, we map bone, cartilage, and stromal development from a population of highly pure, postnatal skeletal stem cells (*m*ouse *s*keletal *s*tem *c*ells, mSSCs) to their downstream progenitors of bone, cartilage, and stromal tissue. We then investigated the transcriptome of the stem/progenitor cells for unique gene-expression patterns that would indicate potential regulators of mSSC lineage commitment. We demonstrate that mSSC niche factors can be potent inducers of osteogenesis, and several specific combinations of recombinant mSSC niche factors can activate mSSC genetic programs in situ, even in nonskeletal tissues, resulting in de novo formation of cartilage or bone and bone marrow stroma. Inducing mSSC formation with soluble factors and subsequently regulating the mSSC niche to specify its differentiation toward bone, cartilage, or stromal cells could represent a paradigm shift in the therapeutic regeneration of skeletal tissues.

INTRODUCTION

Stem cell regulation in the skeletal system, as compared to the hematopoietic system, remains relatively unexplored. Pioneering studies by Friedenstein et al. established the presence of colony-forming skeletogenic cells, but only recently have efforts begun to identify and isolate bone, cartilage, and stromal progenitors for rigorous functional characterization (Bianco, 2011; Chan et al., 2013; Friedenstein et al., 1987; Méndez-Ferrer et al., 2010; Morrison et al., 2006; Park et al., 2012). In addition, the bone marrow is a favored site of prostate and breast cancer metastasis, and the characteristics of the bone stroma supporting metastatic stem cell niches are largely uncharted. Another important challenge in tissue regeneration is the limited capacity to (re)generate cartilage, which is deficient in many diseases (e.g., osteoarthritis, connective tissue disorders) (Burr, 2004; Kilic et al., 2014).

We hypothesized that the skeletal system follows a program similar to that of hematopoiesis, with a multipotent stem cell generating various lineages in a niche that regulates differentiation. Thus we sought to (1) identify a multipotent skeletal stem cell and map its relationship to its lineage-committed progeny and (2) identify cells and factors in the skeletal stem cell niche that regulate its activity.

RESULTS

Identification of the Skeletal Stem Cell, Its Progeny, and Their Lineage Relationships

Bone and Cartilage Are Derived from Clonal, Lineage-Restricted Progenitors

We used a "Rainbow mouse" (Ueno and Weissman, 2006) model to evaluate clonal-lineage relationships in vivo to determine whether mesenchymal tissues in bone—including stroma, fat, bone, cartilage, and muscle—share a common progenitor (Rinkevich et al., 2011) (see Experimental Procedures). To visualize clonal patterns within all tissues, we crossed Rainbow mice with mice harboring a tamoxifen (TMX)-inducible ubiquitously expressed Cre under the actin promoter (Actin-Cre-ERT) (Figure 1C). Six weeks after this recombinase activation, clonal regions could be detected as uniformly labeled areas of a distinct color (Figures S1A and S1B). Using this system, we observe clonal regions in the bone, particularly at the growth plate, that encompass bone, cartilage, and stromal tissue but not hematopoietic, adipose, or muscle tissue at all time points studied (Figures 1A, 1C–1D, and S1D). These data indicate that bone, cartilage, and stromal tissue are clonally derived in vivo from lineage-restricted stem and progenitor cells that do not also give rise to muscle and fat, at least at the time points examined (Figure S1).

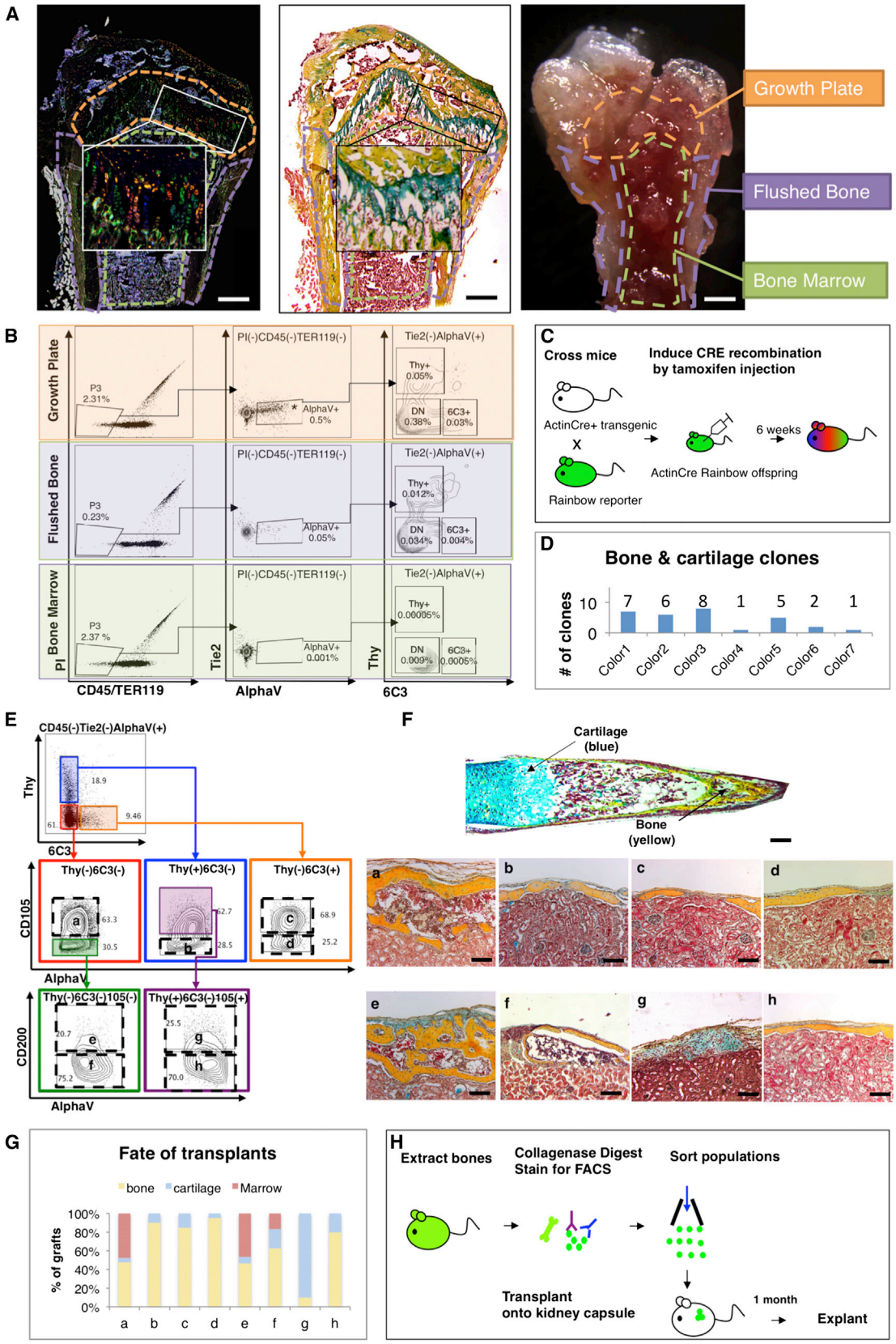

(legend on next page)

Purified Cartilage, Bone, and Stromal Progenitor Cells Are Heterogeneous and Lineage Restricted

As we had observed a high frequency of clonal regions in the growth plate during our Rainbow clonal analysis, we isolated cells from the femoral growth plates by enzymatic and mechanical dissociation and analyzed them by fluorescence-activated cell sorting (FACS) for differential expression of CD45, Ter-119, Tie2, and AlphaV integrin. These surface markers correspond to those present on hematopoietic (CD45, Ter-119), vascular and hematopoietic (Tie2), and osteoblastic (AlphaV integrin) cells. We found that the growth plate had a high frequency of cells that were CD45$^-$Ter-119$^-$Tie2$^-$AlphaV$^+$, hereafter referred to as [AlphaV$^+$]. Based on subsequent microarray analysis of [AlphaV$^+$] showing differential expression of CD105, Thy, 6C3, and CD200, we fractionated this population into eight subpopulations (Figures 1B and 1E) (Seita et al., 2012).

To evaluate the intrinsic ability of the eight subpopulations to give rise to skeletal tissue, we isolated cells of each subpopulation from the long bones, ribs, and sternum of GFP$^+$ mice **(**Figure 1E**)** and transplanted them beneath the renal capsules of immunodeficient mice (Figure 1H). Four weeks after transplantation, we explanted the GFP-labeled kidney grafts and processed the tissues for histological analysis to determine developmental outcome (Figure 1F). The eight subpopulations exhibited different developmental fates (Figures 1F and 1G): three followed a pattern of endochondral ossification (grafts consisting of bone, cartilage, and marrow) (Figures 1F and 1G: populations a, e, f); four gave rise to primarily bone with minimal cartilage and no marrow (Figures 1F and 1G: populations b, c, d, h); and one gave rise to predominantly cartilage with minimal bone and no marrow (Figures 1F and 1G: population g). Unlike the eight subpopulations of [AlphaV$^+$], the CD45/Ter-119$^+$ and Tie2$^+$ subsets did not form bone, cartilage, or stroma (Figure S4), further emphasizing the existence of distinct progenitors of bone, cartilage, and stromal tissue. These results indicate that the skeletogenic progenitors are diverse, with distinct cell-surface marker profiles and skeletal tissue fates, similar to the diverse hematopoietic progenitor cells that generate various differentiated blood cells.

Identification of a Postnatal Skeletal Stem Cell

We hypothesized that skeletogenesis may proceed through a developmental hierarchy of lineage-restricted progenitors as occurs in hematopoiesis. We observed that the [CD45$^-$Ter-119$^-$Tie2$^-$AlphaV$^+$Thy$^-$6C3$^-$CD105$^-$CD200$^+$] subpopulation generates all of the other (seven) subpopulations through a sequence of stages both in vitro and in vivo, beginning with generation of two multipotent progenitor cell types: first, the [CD45$^-$Ter-119$^-$Tie2$^-$AlphaV$^+$Thy$^-$6C3$^-$CD105$^-$CD200$^-$] cell population, hereafter referred to as the pre-BCSP (*pre-b*one *c*artilage and *s*tromal *p*rogenitor); and the [CD45$^-$Ter-119$^-$Tie2$^-$AlphaV$^+$Thy$^-$6C3$^-$CD105$^+$] cell population, which we previously described as the BCSP (*b*one, *c*artilage, and *s*tromal *p*rogenitor) (Chan et al., 2013). The [CD45$^-$Ter-119$^-$Tie2$^-$AlphaV$^+$Thy$^-$6C3$^-$CD105$^-$CD200$^+$] subpopulation generates in vitro and in vivo all of the other (seven) subpopulations in a linear fashion. In vitro, freshly sorted cells were cultured for 25 days, at which point they were refractionated by FACS (Figure 2A (i), Figures 2Bi and 2Bii), and subsequently transplanted beneath the renal capsule (Figures 2Ai and 2Biii). In vivo, the purified cells were transplanted beneath the renal capsule and explanted 1 month later for FACS analysis (Figures 2Aii, 2Ci, and 2Cii) or immunohistochemistry (Figure 2Ciii). These data demonstrate that the [CD45$^-$Ter-119$^-$Tie2$^-$AlphaV$^+$Thy$^-$6C3$^-$CD105$^-$CD200$^+$] subpopulation generates all of the other (seven) subpopulations in a linear fashion both in vitro and in vivo.

Single sorted cells from the [CD45$^-$Ter-119$^-$AlphaV$^+$Thy$^-$6C3$^-$CD105$^-$CD200$^+$] subpopulation also generated all of the other subpopulations in a linear fashion both in vitro and in vivo (Figures 2D and 2E). In vitro: Individual [CD45$^-$Ter-119$^-$Tie2$^-$AlphaV$^+$Thy$^-$6C3$^-$CD105$^-$CD200$^+$] cells were plated and cultured for 14 days (Figure 2Ei). FACS analysis of the resultant primary colonies showed that they contained clones of the original cell and all other (seven) subpopulations of [AlphaV$^+$] (Figure 2Eiv: *middle panel FACS plot*). These colonies contained both cartilage and bone tissue when examined by immunohistochemistry (Figure 2Eiii). Furthermore, when a single freshly sorted [CD45$^-$Ter-119$^-$Tie2$^-$AlphaV$^+$Thy$^-$6C3$^-$CD105$^-$CD200$^+$] cell isolated from the primary colony was again plated

Figure 1. Bone and Cartilage Are Derived from Clonal, Lineage-Restricted Progenitors

(A) Micrographs: 6-week-old Rainbow Actin-Cre-ERT mouse femur, following TMX induction at P3, shows clonal expansion at the growth plate. Fluorescent microscopy (left), pentachrome stain (middle), and dissection microscope (right). Scale bar: 500 μm. Representative of 10 replicates.

(B) FACS plots: cells isolated from three different parts of the femur illustrate that [AlphaV$^+$] is most prevalent in the growth plate (uppermost horizontal panel in the middle) ($p < 0.001$, ANOVA, $n = 3$). DN = double negative, negative for Thy and 6C3 surface expression.

(C) Scheme of experiment: Actin-Cre-ERT transgenic mouse was crossed with Rainbow reporter gene mouse. Cre recombination of offspring was induced by TMX induction on E15, P3, and postnatal week 6. Bones were harvested 6 weeks post-induction.

(D) Graphic representation illustrating different numbers of clones present, which span the bone and cartilage. Representative of sections with ten mice. See also Figure S1.

(E) FACS gating strategy for isolation of eight distinct skeletal tissue subpopulations obtained from the [AlphaV$^+$] subset. a = BCSP, b = BLSP, c = 6C3, d = HEC, e = mSSC, f = pre-BCSP, g = PCP, h = Thy. Representative of 50 replicates.

(F) P3 Femur stained with Movat's pentachrome (top). Sections stained with pentachrome of tissue grafts following cell transplant beneath the renal capsule (bottom). Populations e (mSSC), f (pre-BCSP), and a (BCSP) can reconstruct entire bone, consisting of bone, cartilage, and a functional marrow cavity. Populations b (BLSP), c (6C3), d (HEC), and h (Thy) formed bone with minimal cartilage. Population g (PCP) formed cartilage with a minimum of bone. Scale bar: 200 μm. Representative of 3–20 experiments.

(G) Graph depicting the percentage tissue composition (bone [yellow], marrow [red], and cartilage [blue]) of each of the explanted grafts a to h. Representative of 3–20 experiments.

(H) Scheme of experiment: 20,000 cells of each subpopulation of [AlphaV$^+$] were isolated from the long bones of GFP-labeled P3 mice using FACS. Purified GFP$^+$ cells were then transplanted beneath the kidney capsules of recipient mice. One month later, the grafts were explanted.

See also Figures S1, S3, S4, and S6.

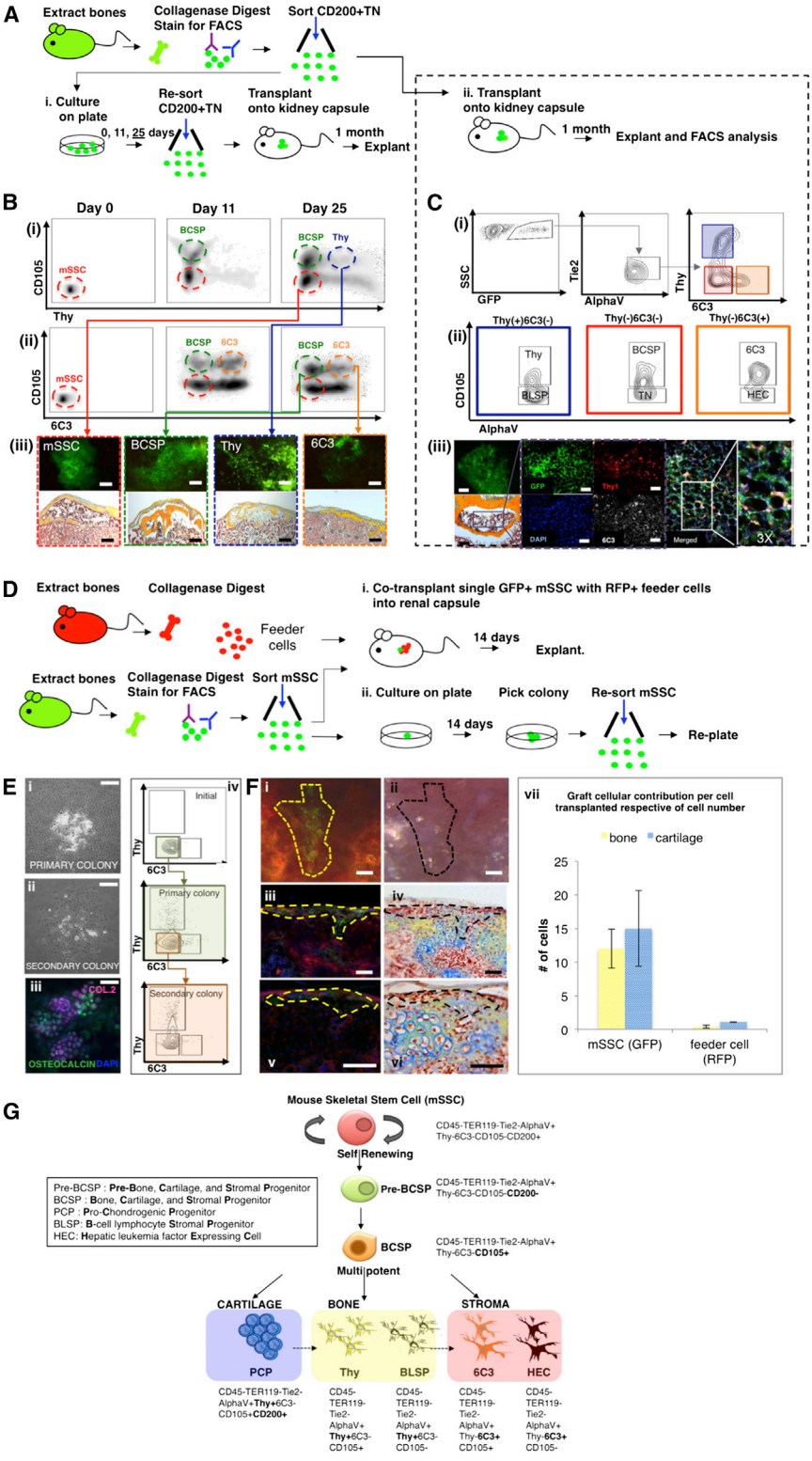

Figure 2. Identification of the mSSC

(A) Scheme of experiment: CD200$^+$TN [CD45$^-$Ter-119$^-$Tie2$^-$AlphaV$^+$Thy$^-$6C3$^-$CD105$^-$CD200$^+$] cells were isolated from femora of GFP$^+$ mice at P3. (i) Purified mSSCs were seeded and harvested on days 0, 11, 25 for FACS analysis. On day 25 following refractionation of the cells by FACS, 20,000 cells of each subset (mSSC, BCSP, Thy, 6C3) were transplanted beneath the kidney capsules of recipient mice. The grafts were explanted 1 month later. (ii) Purified GFP-labeled mSSCs were also directly transplanted beneath the kidney capsules of recipient mice. One month post-transplantation, the grafts were explanted.

(B) FACS analysis of cultured mSSCs on days 0, 11, and 25 in culture (i, ii). Transplanted mSSCs (red box) and BCSPs (green box) formed bone, cartilage, and a marrow cavity. Thy (blue box) and 6C3 (orange box) formed bone only, without a marrow cavity (iii). Scale bar: 500 μm (iii, upper panel), 200 μm (iii, lower panel). Representative of three replicates/subpopulation.

(C) (i, ii) FACS analysis of explanted kidney capsule grafts, in which highly purified populations of GFP-labeled [CD45$^-$Ter-119$^-$Tie2$^-$AlphaV$^+$Thy$^-$6C3$^-$CD105$^-$CD200$^+$] (mSSC) cells were transplanted beneath the kidney capsule: graft consisted of seven downstream subpopulations (blue, red, and orange boxes). Bright-field micrograph of pentachrome-stained explant (iii, far lower left) demonstrates that mSSCs are capable of generating bone, cartilage, and marrow. Immunostained explant (purple box, high magnification) shows that mSSCs are capable of generating cells that express Thy and 6C3 (iii, middle; Thy = red, 6C3 = white). Merged image (iii, extreme right). Fluorescent image of GFP$^+$ graft (iii, far upper left). Scale bar: 500 μm (iii, upper panel), 100 μm (iii, lower panel), 50 μm (iii). Representative of three replicates per transplanted subpopulation.

(D) Scheme of experiment: Unsorted cells from the long bones of RFP$^+$ P3 mice served as feeder cells. Cells from the long bones of P3 GFP$^+$ mice were isolated following mechanical and enzymatic dissociation, and mSSCs were obtained following FACS. (i) A single GFP-labeled mSSC was co-transplanted with 5,000 RFP$^+$ feeder cells beneath the renal capsule of immunodeficient mice. (ii) A single purified GFP-labeled mSSC was plated per well of a 96-well culture dish. Following 14 days, formed colonies were counted, harvested, and re-sorted using FACS, and a single purified GFP-labeled mSSC was again plated per well of a 96-well culture dish, and the assay repeated.

(E) In vitro, colony formation assays were performed by plating a single mSSC in each well of a 96-well culture dish. (i) Representative micrograph of a primary colony depicted at 14 days post-plating. (ii) Passaging of primary colonies resulted in the formation of secondary colonies with similar morphologies to those of primary colonies. (iii) Primary colonies stained positive for anti-collagen 2 (purple), anti-osteocalcin (green), and DAPI (blue) following immunofluorescent staining. (iv) Vertical panel on right depicts FACS analysis of initial mSSC cells isolated (top), subsequent primary colony (middle), and secondary colony cell (bottom). Scale bar: 500 μm (i, ii), 100 μm (iii). Representative of ten assays.

(F) Microscopy of explanted grafts (as per Figure 2Di). The extent of the in vivo colony formation from GFP-labeled mSSCs is outlined by a yellow broken line (i, iii, v) *or* black broken line (ii, iv, vi). Clonally expanded, GFP-labeled mSSCs are seen as green cells (fluorescent image, i, iii, v). Corresponding bright-field

(legend continued on next page)

and cultured for 14 days, the resultant secondary colony contained clones of the original cell and all other subpopulations (Figure 2Eii) on FACS analysis (Figure 2Eiv: *bottom panel FACS plot*). These results demonstrate that the in vitro self-renewal of a single [CD45$^-$Ter-119$^-$Tie2$^-$AlphaV$^+$Thy$^-$6C3$^-$CD105$^-$CD200$^+$] cell maintained the skeletogenic properties of freshly isolated [CD45$^-$Ter-119$^-$Tie2$^-$AlphaV$^+$Thy$^-$6C3$^-$CD105$^-$CD200$^+$] cells. In vivo: When transplanted individually, [CD45$^-$Ter-119$^-$Tie2$^-$AlphaV$^+$Thy$^-$6C3$^-$CD105$^-$CD200$^+$] cells did not engraft efficiently beneath the renal capsule, perhaps reflecting their need for a supportive niche. Thus, we cotransplanted a single GFP-labeled [CD45$^-$Ter-119$^-$Tie2$^-$AlphaV$^+$Thy$^-$6C3$^-$CD105$^-$CD200$^+$] cell with 5,000 unsorted, RFP-labeled cells isolated from the long bones to simulate a niche (Figure 2Di). Two weeks after transplantation, we explanted the grafts for immunohistochemical analysis. The GFP-labeled transplanted cells (Figures 2Fi and 2Fii) differentiated into both chondrocytes and osteocytes in vivo (Figures 2Fiv, 2Fvi, and 2Fvii), consistent with in vitro properties (Figure 2Eiii). These data indicate that the [CD45$^-$Ter-119$^-$Tie2$^-$AlphaV$^+$Thy$^-$6C3$^-$CD105$^-$CD200$^+$] population possesses definitive stem cell-like characteristics of self-renewal and multipotency. We therefore conclude that the [CD45$^-$Ter-119$^-$Tie2$^-$AlphaV$^+$Thy$^-$6C3$^-$CD105$^-$CD200$^+$] cell population represents a *m*ouse *s*keletal *s*tem *c*ell (mSSC) population in postnatal skeletal tissues (Figure 2G), and that the seven other subpopulations of [AlphaV$^+$] are mSSC progeny.

Based on the analyses described above, we defined a lineage tree of skeletal stem/progenitor cells (Figure 2G). The mSSC initiates skeletogenesis by producing a hierarchy of increasingly fate-limited progenitors. The multipotent and self-renewing mSSC first gives rise to multipotent progenitors, pre-BCSPs and BCSPs. These cells then produce the following oligolineage progenitors: pro-chondrogenic progenitors (PCPs) [CD45$^-$Ter-119$^-$Tie2$^-$AlphaV$^+$Thy$^+$6C3$^-$CD105$^+$CD200$^+$]; the Thy subpopulation, [CD45$^-$Ter-119$^-$Tie2$^-$AlphaV$^+$Thy$^+$6C3$^-$CD105$^+$], hereafter referred to as Thy; B cell lymphocyte stromal progenitors, BLSPs [CD45$^-$Ter-119$^-$AlphaV$^+$Thy$^+$6C3$^-$CD105$^-$]; the 6C3 subpopulation, [CD45$^-$Ter-119$^-$AlphaV$^+$Thy$^-$6C3$^+$CD105$^+$], hereafter referred to as 6C3; and the hepatic leukemia factor-expressing cell, HEC [CD45$^-$Ter-119$^-$AlphaV$^+$Thy$^-$6C3$^+$CD105$^-$] (Figure 2G). mSSC-derived lineages include cell types that we have previously characterized, which possess distinct hematopoietic supportive capabilities (Chan et al., 2013) (Figures S2A and S2B).

Identification of Factors that Regulate Skeletal Stem and Progenitor Cell Activity and Differentiation

Downstream Skeletal Progenitors Regulate mSSC Activity

Once we had isolated the mSSC, we focused on identifying the cells that make up the mSSC niche, the microenvironment that supports and regulates stem cell activity. We first conducted microarray gene-expression analyses of freshly sorted mSSC/pre-BCSP and five downstream progenitor populations [(1) BCSP; (2) Thy; (3) 6C3; (4) BLSP; and (5) HEC] to identify receptors to signaling pathways that may regulate activity of the mSSC and its progeny (Figures 3D and 3E).

To interpret the gene-expression profiles of these cells, we used the Gene Expression Commons (Seita et al., 2012), a platform that normalizes microarray data against a large collection of publicly available microarray data from the National Center for Biotechnology Information Gene Expression Omnibus. From this analysis, it is apparent that mSSC and its progeny differentially express receptors involved in transforming growth factor, *TGF* (specifically bone morphogenetic protein [*BMP*]) and *Wnt* signaling pathways, and cognate morphogens of these pathways, including *BMP2*, *TGF-β3*, and *Wnt3a* (Figures 3D and 3E). These results suggest that paracrine and/or autocrine signaling among mSSCs and their progeny may positively regulate their own expansion (Figure 3F). Furthermore, single cell RNA sequencing revealed coexpression of BMP2 and its receptor (*BMPR1a*) in 28% of mSSCs (Figures 3A–3C and S5), supporting potential for autocrine and/or paracrine signaling in the mSSCs.

In support of transcriptional data, the addition of exogenous recombinant BMP2 to culture media rapidly induced expansion of isolated mSSC, whereas supplementation of media with either exogenous recombinant TGF-β or tumor necrosis factor alpha (TNF-α) did not (Figures 3G and 3H). In addition, proliferation of mSSC in vitro was markedly inhibited by addition of recombinant gremlin 2 (an antagonist of BMP2 signaling) protein to culture media, in contrast to control. Progeny of the mSSCs express antagonists of the BMP2 signaling pathway, such as *Gremlin 2* and *Noggin* (Figure 3I), suggesting the presence of a potential negative feedback mechanism to control mSSC proliferation by more differentiated progeny. Specifically, Thy expresses *Gremlin 2*, and both Thy and BLSP express *Noggin*. This is consistent with Thy and BLSP subpopulations acting in a negative feedback loop to inhibit BMP2-induced proliferation of the mSSC, further supporting a regulatory role for paracrine signaling among mSSCs and their progeny.

Shifting Fates: Cartilage to Bone

Our next step was to comprehend signaling pathways that could play a role in directing the differentiation of skeletal stem/progenitor cells. Specifically, we wished to direct osteogenesis to chondrogenesis, as this is directly related to a large unmet clinical need for cartilage (Bhumiratana et al., 2014; Jo et al., 2014; Makris et al., 2014; Mollon et al., 2013). We asked whether mSSC-derived stroma could influence fate commitment of skeletal progenitor cells (Figure 2G). We observed that the skeletal subsets with the immunophenotype [CD45$^-$Ter-119$^-$AlphaV$^+$Thy$^+$6C3$^-$CD105$^+$CD200$^+$] (Figure 1F: population g) isolated

micrographs are shown (ii, iv, vi). Fluorescent imaging of transverse sections of grafts are shown (iii, v). Corresponding bright-field micrographs of pentachrome-stained sections demonstrate that clonally expanded cells are fated into bone (yellow) and cartilage (blue) (iv, vi). Graph (vii) is representative of the contribution by GFP or RFP cells (per cell transplanted) to bone or cartilage formation (mean ± SEM). Scale bar: 200 μm (i–vi). Representative of five transplants of each assay. (G) Schematic representation of the skeletal stem cell lineage tree. The mSSC occupies the apex of this hierarchal tree and is multipotent and capable of self-renewal and differentiation into more lineage-restricted progenitor cells (pre-BCSP and BCSP). The mSSCs, pre-BCSPs, and BCSPs are capable of giving rise to bone, cartilage, and hematopoietic supportive stroma. The immunophenotype of each cell is shown.

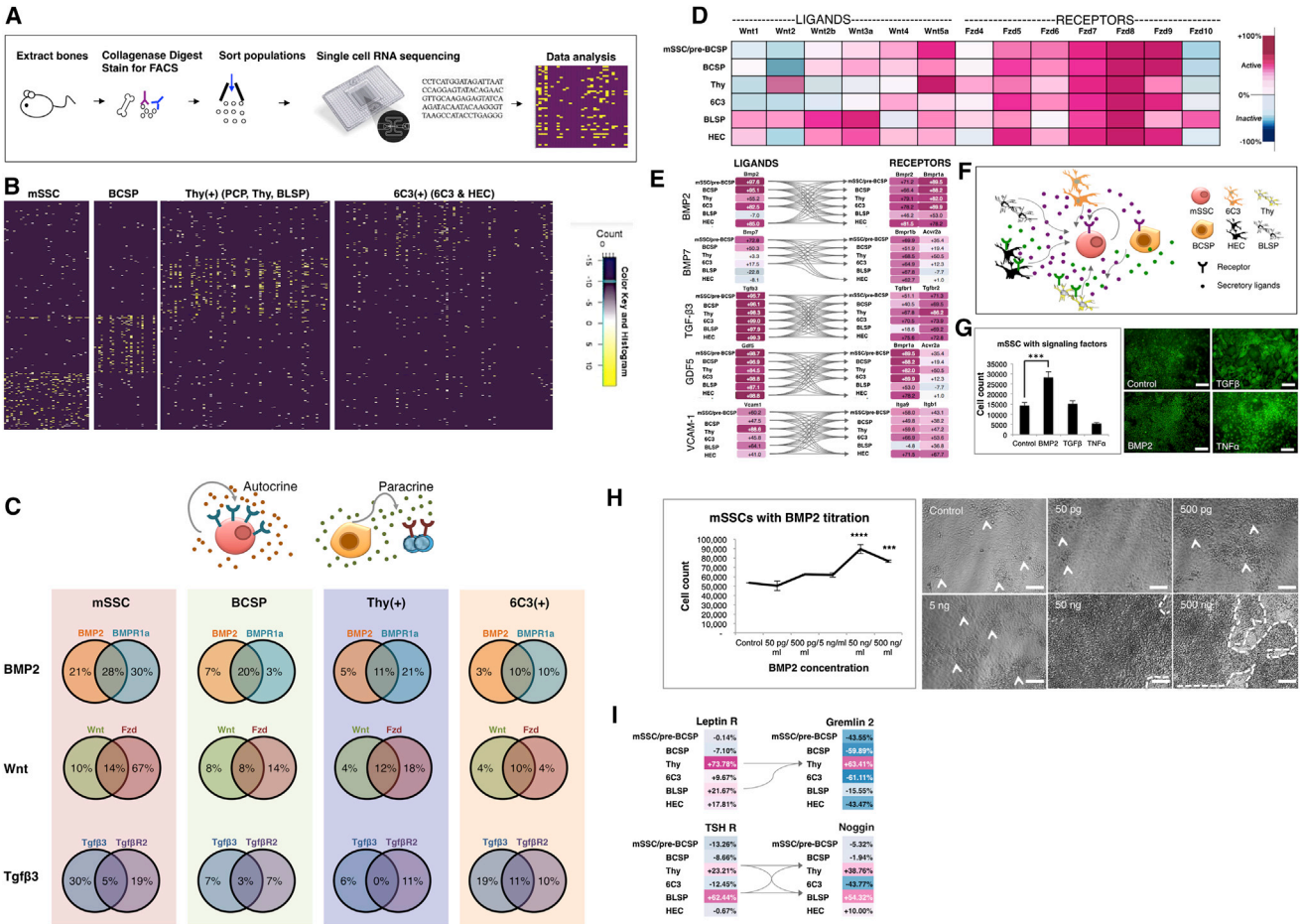

Figure 3. The mSSC Niche Is Composed of Other Skeletal-Lineage Cells

(A) Scheme of experiment: Long bones of P3 mice were harvested as previously described. The cell suspension was sorted by FACS to obtain mSSC; BCSP; Thy$^+$, which encompasses the PCP, Thy, and BLSP subsets; and 6C3$^+$, which encompasses 6C3 and HEC. Cell subpopulations were prepared for single-cell RNA sequencing.

(B) Hierarchical clustering of single-cell RNA-sequencing data demonstrates four molecularly distinct patterns of single-cell transcriptional expression between mSSC, BCSP, Thy$^+$, and 6C3$^+$.

(C) Percentage transcriptional expression of morphogen (left circle in each Venn diagram), receptor (right circle in each Venn diagram), or both (overlapping central portion of the Venn diagram) on single-cell RNA sequencing. Note that the percentage denotes the percentage of cells within each subset (mSSC, BCSP, Thy$^+$, and 6C3$^+$), which express the relevant gene sequence. (Top) The patterns show the potential for paracrine (right) and autocrine (left) signaling.

(D) Gene-expression levels of Wnt-associated genes in skeletal populations as determined using the Gene Expression Commons analysis platform. The range of transcriptional expression is illustrated by a color change as depicted on the extreme right of the figure (i.e., dark purple correlates to high expression, whereas dark blue correlates to low expression). Heatmap shows high expression of both Wnt ligands (*Wnt3a*, *Wnt4*, *Wnt5a*) and receptors (*Fzd5-9*), demonstrating that Wnt signaling may be actively involved in skeletal progenitor function. Fzd = frizzled receptor. These data were compiled in triplicate, with 10,000 cells of each subset analyzed in each sample.

(E) Ligand-receptor interaction maps demonstrate that the skeletal stem/progenitor cells can act as their own niche and signal through each other to promote skeletogenesis. Gene-expression analysis of microarray data extracted from skeletal subsets show ligands in the left column and cognate receptors in the right column. The connecting arrows indicate possible ligand-receptor interaction pathways. Note: GDF = growth and differentiation factor, VCAM-1 = vascular cell adhesion molecule-1. Data were compiled from triplicate samples, with 10,000 cells of each subset analyzed in each sample.

(F) Diagram illustrating potential signaling pathways influencing activity of skeletal stem/progenitor cells. Paracrine and/or autocrine signaling may occur in the skeletal stem cell niche and regulate cell activity and maintenance.

(G) Fluorescent micrographs illustrate colony morphology of mSSCs post-culture with morphogen (BMP2/TGF-β/TNF-α) supplementation/control (right). Graph shows the number of mSSCs present following culture for 14 days under the different conditions (left). rhBMP2 supplementation was associated with significant amplification of the mSSC populations in vitro (bottom left) in comparison to control, nonsupplemented media (top left) (mean ± SEM, $p < 0.01$, t test, $n = 3$). Supplementation with TGF-β or TNF-α resulted in altered colony morphology (upper and lower right). These results show that niche signaling can influence mSSC proliferation. Scale bar: 200 μm.

(H) Graph illustrates the effect of rhBMP2 titration on mSSC proliferation in culture (left). The effect of BMP2 was significantly greater than control at each of the following concentrations: 50 ng/ml (mean ± SEM, $p < 0.001$, *ANOVA*), 500 ng/ml (mean ± SEM, $p < 0.01$, *ANOVA*). Phase images illustrate the colonies of cells

(legend continued on next page)

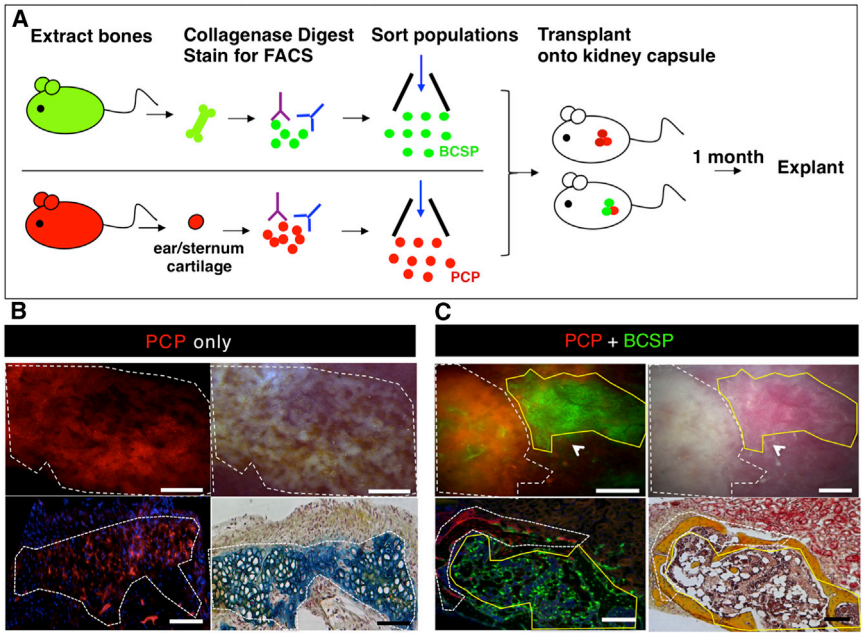

Figure 4. Shifting Fates: Cartilage to Bone

(A) Scheme of experiment: BCSPs were isolated from femora of GFP$^+$ mice at P3, and PCPs were isolated from ears/sternum of RFP$^+$ adult mice following mechanical and enzymatic digestion and subsequent FACS fractionation. Purified GFP$^+$ BCSP and RFP$^+$ PCP were cotransplanted beneath the kidney capsules of immunodeficient recipient mice. RFP$^+$ PCP transplant served as a control. One month after transplantation, all grafts were removed for analysis.

(B) Microscopy of explanted grafts 1 month following transplantation of 20,000 RFP$^+$ PCP cells (see Figure 4A). The white dotted line outlines the extent of the graft formed. Fluorescence micrograph of explanted graft demonstrate the presence of an RFP$^+$ graft (upper left). Corresponding bright-field micrograph is shown in upper right panel. Transverse section stained with Movat's pentachrome demonstrates that RFP-labeled PCP cells form cartilage (blue stain) (lower right). Scale bar: 500 μm (upper panel), 200 μm (lower panel). Representative of four replicates.

(C) Microscopy of explanted grafts following co-transplantation of 20,000 RFP-labeled PCP cells with 20,000 GFP-labeled BCSPs (as detailed in Figure 4A). The grafts, which formed, are outlined by a white dotted line (indicating RFP$^+$ portion) and a yellow solid line (indicating GFP$^+$ portion) (upper left). A corresponding bright-field micrograph is shown in the upper right panel. A transverse section stained with Movat's pentachrome shows that both RFP-labeled PCPs and GFP-labeled BCSPs form bone (yellow stain) (lower right). Scale bar: 500 μm (upper panel), 200 μm (lower panel). Representative of five replicates.

from RFP$^+$ mice are directed primarily toward cartilage formation when transplanted in isolation beneath the renal capsule of nonfluorescent mice; thus, we designated this cell the PCP (Figures 4A and 4B). However, when RFP-labeled PCPs (Figure 2G) are cotransplanted with GFP-labeled BCSPs, they differentiate into bone but not cartilage (Figure 4C).

Shifting Fates: Bone to Cartilage

Having observed that signaling from cotransplanted BCSP could divert cartilage-fated cells toward bone formation, we next sought to identify factors that could, conversely, selectively promote mSSCs to cartilage rather than bone fates. Emerging evidence indicates that increased VEGF expression can spur resting chondrocytes to re-enter a hypertrophic state and resume endochondral ossification (Saito et al., 2010; Street et al., 2002). Thus, we aimed to determine whether inhibition of VEGF signaling could promote chondrogenic differentiation of mSSCs by blocking VEGF-dependent ossification (Figure 5A). We administered adenoviral vectors encoding a soluble ligand-binding ectodomain (ECD) of the VEGFR1 receptor (Ad sVEGFR1) intravenously, leading to potent systemic VEGF antagonism (Wei et al., 2013). Adenovirus encoding a control immunoglobulin IgG2α Fc domain served as control treatment. One day later, we transplanted either intact embryonic day (E) 14.5 pre-osteogenic fetal femora or freshly sorted mSSCs under the renal capsules of these mice and then explanted the tissue 3 weeks later (Figure 5A). The grafts from the Ad sVEGFR1-treated mice contained predominantly cartilaginous tissue (Figure 5B, right). In contrast, the grafts from the control Ad Fc animals evidenced endochondral ossification and formation of a marrow cavity surrounded by cortical bone (Figure 5B, left). These results suggest that VEGF blockade may promote chondrogenesis at the expense of osteogenesis (Figure 5C).

BMP Pathway Manipulation Can Induce De Novo Formation of the mSSC in Extraskeletal Locations

We next investigated whether other tissue types contain cells that are osteo-inducible or harbor dormant mSSCs that can be activated to undergo osteogenesis. As we observed that BMP2 can expand mSSC in vitro (Figures 3G and 3H), we tested BMP2 as an agent that may induce such osteogenesis. We placed collagen sponges containing recombinant BMP2 into subcutaneous extraskeletal sites. Harvest of the collagen sponges 4 weeks after placement revealed abundant osseous

derived from the mSSCs (indicated by arrowhead in control, 50 pg/ml, 500 pg/ml, 5 ng/ml and by a broken line in 50 ng/ml and 500 ng/ml) (right). Scale bar: 500 μm, n = 3.

(I) Ligand-receptor interaction maps show gene-expression levels of BMP antagonists gremlin 2 and Noggin (right top and bottom, respectively). There is increased expression of the receptors for the systemic hormones leptin and thyroid-stimulating hormone (TSH) on the same subpopulations of downstream progenitors Thy and BLSP (left top and bottom), which express BMP antagonists. Viewing the left and right panels in unison, the ligand-cognate receptor interaction graph shows that signaling through systemic hormones leptin and TSH receptors may produce inhibitory signals for mSSC expansion by BMP2 antagonism (via gremlin 2, noggin) and subsequent osteogenesis in skeletal stromal populations. Arrows illustrate the potential receptor-ligand interactions. Data were compiled from triplicate samples, with 10,000 cells of each subset analyzed in each sample.

See also Figures S2 and S5.

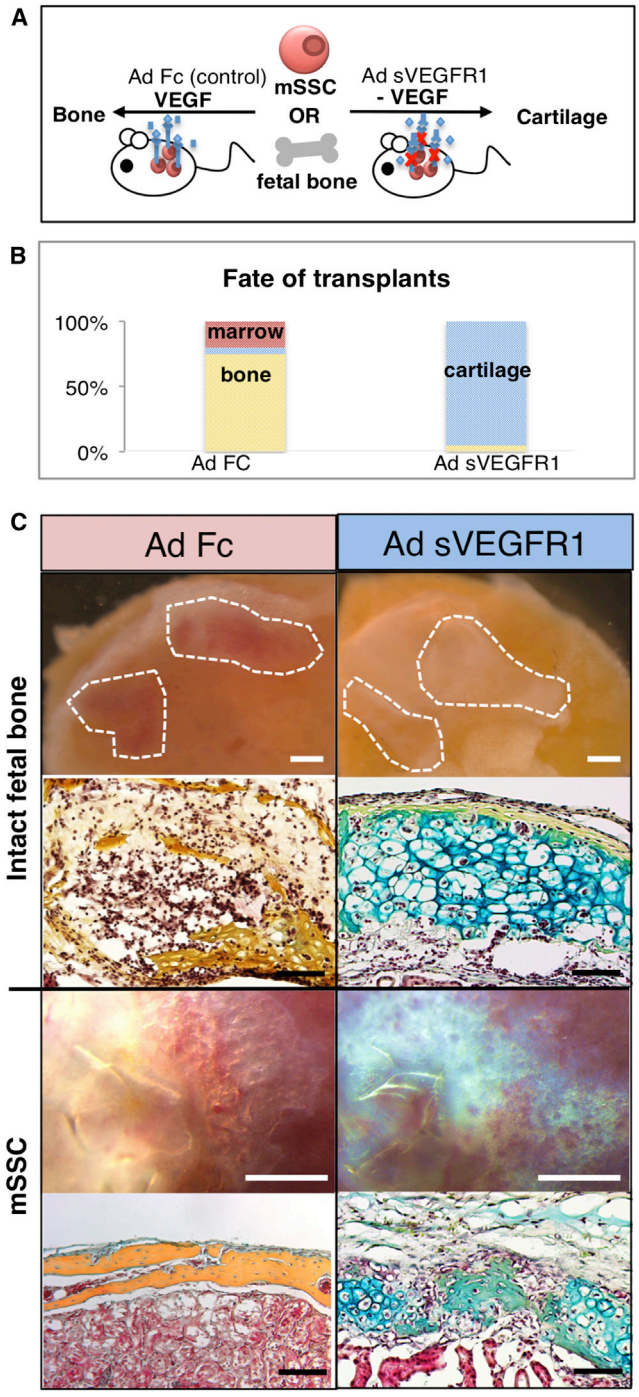

Figure 5. Shifting Fates: Bone to Cartilage

(A) Scheme of experiment: mSSCs were isolated from P3 mice as described previously. Either intact pre-osteogenic femora isolated from E14.5 mice or 20,000 mSSCs were then transplanted beneath the kidney capsules of recipient mice with/without systemic inhibition of VEGF signaling. For inhibition of VEGF signaling, adenoviral vectors encoding soluble VEGFR1 ectodomain (Ad sVEGFR1) were delivered intravenously to the recipient mice 24 hr prior to cell transplantation, leading to systemic release of this potent antagonist of VEGF signaling. Ad Fc encoding an immunoglobulin Fc fragment was served as a negative control. Grafts were explanted 3 weeks later.

osteoids replete with marrow (Figures 6A–6C). Furthermore, FACS analysis of cells within the marrow of the induced osteoids revealed that hematopoietic stem cell (HSC) engraftment also occurs in the osteoids (Figure 6B). By FACS analysis, we determined that mSSCs are normally not detectable or are exceedingly rare in subcutaneous adipose tissue (Figure 6C, right panel). In contrast, mSSCs are plentiful in BMP2-induced osteoids 10 days after implantation, whereas ossification is still proceeding (Figure 6C, left panel).

To determine whether BMP2 induced skeletal transformation of in situ cells or migration of circulating skeletal progenitors recruited from bone tissue, we used a parabiont model (Figure 6D). We surgically fused actin-GFP transgenic mice to non-GFP congenic mice such that they established a shared circulatory system (Conboy et al., 2013). Two weeks after parabiosis, after confirmation of chimerism, we implanted collagen sponges containing recombinant BMP2 into the inguinal fat pad of the non-GFP parabiont. Ten days after implantation, we explanted the sponge and surrounding tissue and performed mechanical and chemical dissociation to isolate the constituent cells. We assayed the contribution of the GFP-labeled cells to ectopic bone formation in the non-GFP mouse by FACs analysis to determine whether circulating cells contributed to ectopic bone development. The tissue of the explants contained abundant GFP-labeled cells at harvest, but GFP-labeled cells in the graft were solely $CD45^+$ hematopoietic cells (Figure 6D, left panel, top and bottom) and not skeletal progenitors (Figure 6D, FACS plots, mSSC cell population shown on far right). The skeletal progenitor population present in the explanted tissue was entirely GFP negative, suggesting that circulating cells did not contribute to BMP2-induced ectopic bone. These data indicate that BMP2-induced osteogenesis involves local cell response that is sufficient to induce mSSC formation in the subcutaneous fat pads, leading to formation of ectopic bone that can support hematopoiesis.

We next wished to determine which cell types could undergo BMP2-mediated reprogramming to mSSC in these extraskeletal sites. We, therefore, conducted FACS analysis of suspended cells isolated from the kidney and the subcutaneous adipose tissue and looked for markers that could distinguish cell types common to both of these extraskeletal organs. We found that both kidney and adipose tissue contain high numbers of Tie2 (Arai et al., 2004; De Palma et al., 2005; Heldin and Westermark, 1999). Using a specific Tie2Cre × MTMG reporter mouse, which genetically labels cells that expressed Tie2 with GFP and other cells with RFP, we again inserted collagen sponges containing

(B) Graphic representation of the fate of the mSSC/fetal bone transplants in the presence of Ad sVEGFR1 or Ad Fc control. Cartilaginous fate is promoted in the presence of systemic VEGF antagonism (n = 5, *ANOVA*, $p < 0.001$).

(C) Explanted grafts are shown in the first and third rows from the top of the panel (control, Ad Fc in left panel, and Ad sVEGFR1 in the right panel). Representative sections stained with Movat's pentachrome are shown in the second and fourth rows from the top of the panel (top two rows: intact fetal bone, bottom two rows: mSSC). VEGF signaling inhibition resulted in the formation of cartilage (blue stain) (right), with the Ad Fc group forming bone (yellow stain) (left). Scale bar: 500 μm (intact fetal bone, top), 100 μm (intact fetal bone, bottom), 500 μm (mSSC, top), 200 μm (mSSC, bottom). Representative of five replicates per assay.

recombinant BMP2 into the inguinal fat pad and harvested the implanted tissue 1 month later (Figure 6E). FACS analysis revealed that BMP2-derived ossicles clearly incorporated GFP-positive Tie2-derived osteocytes with visible canaliculi (Figure 6F, high-magnification inset) and Tie2-negative RFP-labeled osteocytes (Figure 6F), suggesting that both Tie2-positive and Tie2-negative lineages underwent BMP2-induced skeletal reprogramming. These data suggest that a variety of cell types could potentially be induced by BMP2 to initiate formation of mSSC.

Codelivery of BMP2 and VEGF Inhibitor Is Sufficient to Induce De Novo Formation of Cartilage in Adipose Tissue

Although bone itself possesses regenerative ability, the capacity for regeneration in other skeletal tissue (e.g., cartilage) is very low. As BMP2 induction could stimulate mSSC expansion and formation (Figures 3G, 3H, and 6C), we speculated that the mSSC-inducing capacity of BMP2 could be coupled with VEGF blockade to direct de novo cartilage formation. To test this possibility, we implanted BMP2-treated collagen sponges into the adipose tissue of mice that had either been treated 24 hr earlier with intravenous Ad sVEGFR1 as in Figure 5 or included soluble VEGFR1 ECD (50 μg) directly in the collagen sponge (Figure 7A). One month later, the tissues were explanted. BMP2 alone generated bone tissue with a marrow cavity (Figure 7B, left panel). However, BMP2 with either systemic or local VEGF inhibition resulted in predominant cartilage formation (Figure 7B, right panel). The induced cartilage contained a similar frequency of PCPs to that seen in natural cartilage (Figure 7C). As native adipose tissue normally does not undergo chondrogenesis, the induced cartilage likely derives from BMP2-induced mSSCs that were shifted toward cartilage fate by the action of VEGF blockade.

Translational Implications of Skeletal Stem Cell Biology

We next investigated the role of mSSCs in skeletal repair. Highlighting their potential regenerative capabilities, we find that the mSSC number is significantly higher in the callus of a fractured femur than in the uninjured femur (Figures S6A and S6B). Interestingly, mSSCs isolated from a fracture callus also demonstrate enhanced osteogenic capacity (in comparison to uninjured) in vitro (Figure S6C, left panel) and in vivo (Figure S6C, right panel). As it is well known that irradiation results in osteopenia and reduced fracture healing (Mitchell and Logan, 1998), we asked whether the skeletal response to irradiation is linked to depletion of mSSC activity. When mice were irradiated 12 hr prior to fracture induction, we noted a significant reduction in mSSC expansion at 1 week following fracture in comparison to nonirradiated femora 1 week post-fracture (Figure S6D), echoing previous observations (Galloway et al., 2009).

DISCUSSION

Identifying Postnatal Skeletal Stem/Progenitor Cells and Defining the Lineage Tree

The mSSC lineage map we present consists of eight different cellular subpopulations with distinct skeletogenic properties and encompasses subpopulations that have characteristics of described skeletogenic cell types identified by lineage tracing (Bianco, 2014, Méndez-Ferrer et al., 2010; Park et al., 2012; Zhou et al., 2014). For example, the Thy subtype selectively expresses high levels of CXCL12, leptin receptor, and nestin, which are characteristics of CXCL12-abundant reticular cells, leptin receptor-expressing cells (LepR$^+$), and Nestin-expressing mesenchymal stem cells, respectively. We also find that both Nestin-cre- and MX1-cre-labeled populations overlap with the mSSC population (Figure S3) (Chan et al., 2013).

Signals Controlling mSSC and Progenitor Activity

Mechanistically, mSSC expansion and self-renewal must be tightly controlled, evidenced by the expression of numerous cognate receptors to signaling molecules belonging to most of the known signaling pathways, including Hedgehog, BMP, FGF, and Notch. Both BMP2 and 4 are expressed by mSSCs and most mSSC-derived subsets, where they likely mediate survival and expansion via both autocrine and paracrine loops. Conversely, downstream progeny of mSSCs, such as Thy and BLSP populations, express noggin and/or gremlin 2, which antagonize BMP signaling. This suggests that mSSCs and some of their progeny form a portion of their own niche, maintaining critical levels of prosurvival factors such as BMP2 but also controlling skeletal growth by antagonizing BMP signaling. In addition, mSSCs are dramatically amplified in fracture callus, implying that extrinsic signals generated in the regenerative environment could locally activate these cells (Figure S6).

Directing Skeletal Progenitor Fate Determination from Bone to Cartilage

Antagonistic signaling between mSSC-derived skeletal subsets also appears to be a key mechanism in skeletal subset lineage commitment, particularly to either a bone or cartilage fate. When we antagonized VEGF signaling in early skeletal progenitors, bone fates were inhibited in favor of cartilage fates. These results echo previous reports, which suggest that VEGF acts as an essential chondrogenic regulator (Carlevaro et al., 2000; Gerber et al., 1999; Harper and Klagsbrun, 1999).

Directing Skeletal Progenitor Fate Determination from Cartilage to Bone

Paracrine signaling among skeletal subsets may also participate in determining bone versus cartilage formation, specifically in favoring bone. Altered signaling in a particular subpopulation can direct the skeletal fate of other subpopulations in the microenvironment. It is possible that pathological conditions involving calcification of cartilaginous tissues, such as osteoarthritis, could stem from defects in the mSSC niche, leading to aberrant signaling that promotes osteogenesis.

Hematopoietic and Skeletal Stem Cell Homeostasis May Be Closely Related

At a transcriptional level, mSSC-generated progeny express numerous cytokines necessary for HSC maintenance and hematopoiesis, including Kit ligand and stromal-derived factor (Figure S2C). We also find evidence that stem and progenitor cells of the hematopoietic system may reciprocally regulate skeletal progenitors (Figures S2A, S2B, and S2D). We conducted gene-expression analysis of multiple hematopoietic stem and

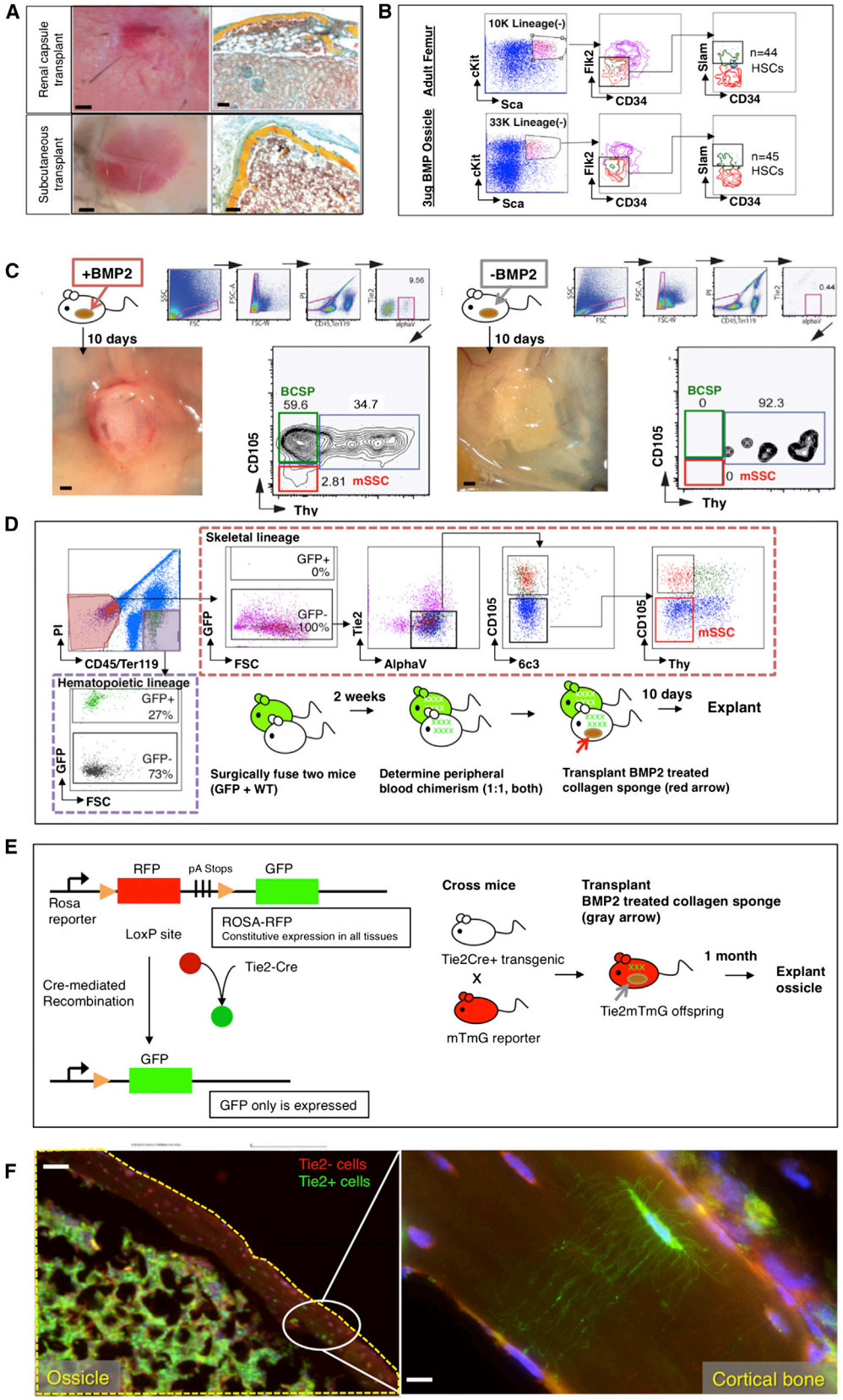

(legend on next page)

progenitor subsets and found that hematopoietic progenitors express myriad factors associated with skeletogenesis, including *BMP2*, *BMP7*, and *Wnt3a*. As previously shown, the cognate receptors of these factors are highly expressed by mSSCs and their progeny (Figures 3D and 3E). Intriguingly, although mSSC-generated progeny, such as Thy and BLSP, selectively express receptors to circulating systemic hormones, such as leptin and thyroid-stimulating hormone, these receptors are not highly expressed in HSCs or hematopoietic subsets (Figure S2D; data not shown; Seita et al., 2012), thus, suggesting that mSSC-derived stromal cells may link systemic endocrine regulation to both skeletal and hematopoietic systems.

Altering Extraskeletal Niche Signaling to Induce Osteogenesis and Chondrogenesis

Modulating niche signaling can stimulate tissue growth by inducing proliferation of stem cells, as we have observed with skeletal stem cells and as described in the hematopoietic system (Calvi et al., 2003). Niche interactions may also play significant roles in maintaining lineage commitment, for instance, high levels of BMP2 signaling can dominate local adipose signaling and re-specify resident Tie2$^+$ and Tie2$^-$ subsets to undergo osteogenesis. Niche interactions can also determine the fate of the mSSC. By implanting BMP2-treated collagen sponges in concert with systemic or local application of soluble VEGF receptor, we demonstrate that cartilage can be induced to form entirely by manipulation of local signaling pathways in extraskeletal tissue.

Conclusion

Inducing mSSC formation with soluble factors and subsequently regulating the mSSC niche to specify its differentiation toward bone, cartilage, or stromal cells could represent a paradigm shift in the therapeutic regeneration of skeletal tissues. This therapeutic modality could also extend to the codependent hematopoietic system even when resident levels of endogenous mSSCs have been depleted by disease or aging. The challenge now is to understand how intrinsic and extrinsic signals guide mSSCs to regulate skeletal shape and patterning at the single-cell level.

EXPERIMENTAL PROCEDURES

Detailed experimental procedures are described in the Extended Experimental Procedures.

Mice

C57BL6, Rag-2/gamma(c)KO, C57BL/6-Tg(CAG-EGFP)1Osb/J, Mx1Cre, and mTmG were bred in our laboratory. Rosa-Tomato Red RFP and Tie2Cre mice were obtained from Jackson. "Rainbow" mice were bred with mice harboring a TMX-inducible ubiquitously expressed Cre under the promoter of the actin gene. Mice were bred at our animal facility according to NIH guidelines. Protocols were approved by the institutional review board.

Isolation and Transplantation of Adult and Fetal Skeletal Progenitors

Skeletal tissues were dissected from postnatal day (P) 3 GFP-labeled mice and dissociated by mechanical and enzymatic dissociation. Total dissociated cells were stained with fluorochrome-conjugated antibodies for fractionation by FACS. Sorted and unsorted skeletal progenitors were then injected under the renal capsule of immunodeficient mice.

Transcriptional Expression Profiling

Microarray analyses was performed on mSSC/pre-BCSPs, BCSPs, Thy$^+$, 6C3$^+$, HEC, and BLSPs. RNA was isolated, twice amplified, streptavidin-labeled, fragmented, and hybridized to Affymetrix 430-2.0 arrays. Raw microarray data were submitted to Gene Expression Commons (http://gexc.stanford.edu). Heatmaps representing fold change of gene expression were generated in Gene Expression Commons.

Histological Analysis of Endochondral Ossification

Representative sections were stained with H&E, Movat's modified pentachrome, or alizarin red stains depending on requirement.

Immunofluorescence

Briefly, specimens were treated with a blocking reagent, then probed with monoclonal antibody at 4°C overnight. Specimens were washed, probed

Figure 6. Manipulation of the BMP Pathway Can Induce De Novo Formation of the mSSCs in Extraskeletal Regions

(A) Collagen sponges containing 3 μg of lyophilized rhBMP2 were placed into extraskeletal sites in C57BL6 wild-type mice. One month later, the graft was explanted for analysis. Bright-field images of explants are shown, with renal capsule transplants shown above and subcutaneous transplants shown below (left). Transverse sections stained with Movat's pentachrome demonstrate that induced osseous osteoids formed a marrow cavity (red stain) (right). Scale bar: 500 μm (left), 200 μm (right). Representative of five replicates.

(B) FACS analysis of cells within the induced osteoid marrow reveals that circulating SlamF1-positive HSC engraftment occurs in the osteoids (bottom row) similar to that which occurs naturally in "normal" adult femurs (top row). Representative of three replicates.

(C) (Left) Following explantation of rhBMP2-laced collagen sponges at day 10 post-extraskeletal placement, FACS analysis of constituent cell populations present within the graft revealed that mSSC (red box on FACS plot) and BCSP (green box on FACS plot) are readily detectable in the rhBMP2-treated explants. (Right) In contrast, FACS analysis of adipose tissue in the absence of BMP2 does not detect either mSSC (red box on FACS plot) or BCSP (green box on FACS plot). Scale bar: 500 μm. Representative of three replicates.

(D) A parabiosis model of GFP$^+$ and non-GFP mouse shows that circulating skeletal progenitor cells did not contribute to BMP2-induced ectopic bones. A GFP$^+$ mouse was parabiosed to a non-GFP mouse. Two weeks later, a collagen sponge containing 3 μg of lyophilized rhBMP2 was transplanted into the inguinal fat pad of the non-GFP mouse. Ten days later, the tissue was explanted and isolated the constituent cell populations of the ectopic bone tissue as described previously. The contribution of the GFP-labeled cells to ectopic bone formation in the non-GFP mouse was analyzed by FACS (broken red line; GFP$^+$ = circulating cells, and nonfluorescent = local cells). GFP-labeled cells contributing to the graft were solely CD45$^+$ hematopoietic cells (extreme left panel, broken purple line) and not consistent of the skeletal progenitor population (horizontal upper panel, mSSCs shown in red box on FACS plot). Representative of three replicates.

(E) (Left) Diagram of reporter gene mouse model shows that Tie2 expression leads to GFP expression. Tie2$^+$ cells turn green, but Tie2$^-$ cells remain red. (Right) Scheme of experiment: In order to determine the cell types, which could undergo BMP2-mediated reprogramming to mSSCs in extraskeletal sites, we implemented a Tie2Cre × MTMG reporter mouse and placed a collagen sponge containing rhBMP2 into the subcutaneous inguinal fat pad. The ossicle was explanted 1 month later for histological analysis.

(F) Fluorescent micrographs: BMP2-derived ossicles (yellow broken line) clearly incorporate both GFP$^+$ Tie2$^+$-derived osteocytes with visible canaliculi and Tie2$^-$ RFP-labeled osteocytes. Area denoted by white oval is shown at higher magnification in the box on the extreme right, showing the presence of GFP$^+$ Tie2$^+$ canaliculi in the presence of RFP$^+$ Tie2$^-$ cells. Scale bar: 500 μm (left), 50 μm (right). Representative of three replicates.

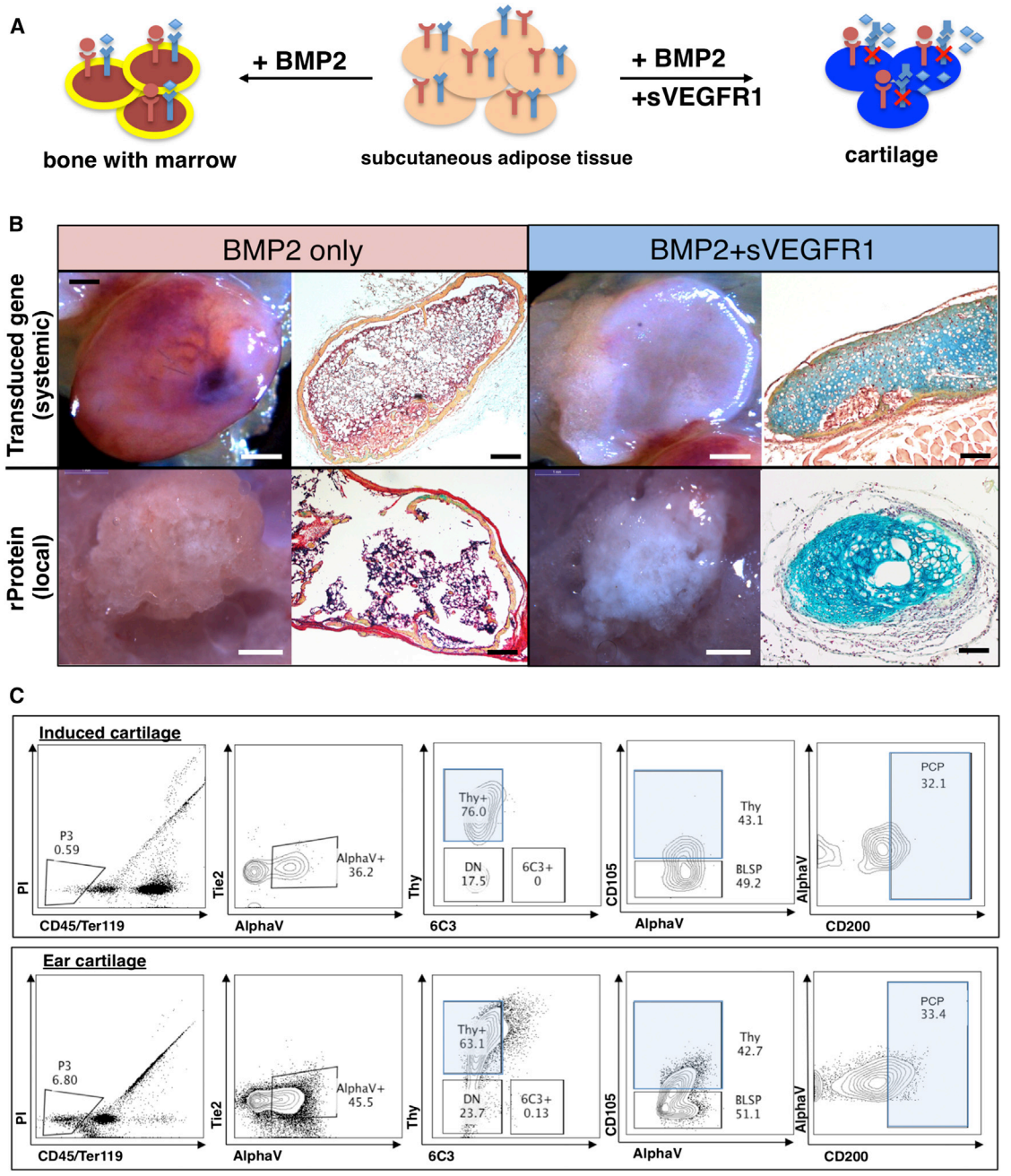

Figure 7. Codelivery of BMP2 and VEGF Inhibitor Is Sufficient to Induce De Novo Formation of Cartilage in Adipose Tissue

(A) Scheme of experiment: codelivery of BMP2 and soluble VEGFR1 in adipose tissue. BMP2 and inhibition of VEGF signaling leads to cartilage formation. BMP2 alone leads to bone formation.

(B) Fate of subcutaneous collagen sponge implants containing BMP2 without (two panels on left) or with VEGF blockade (two panels on right). One month after placement of collagen sponges, the grafts were explanted for analysis. Bright-field images of grafts (left) are shown alongside representative sections stained with Movat's pentachrome (right). The codelivery of BMP2 and sVEGFR1 resulted in the formation of blue staining cartilage (extreme right panels, top and bottom). The result following systemic VEGF blockade is shown in the top series on the right, whereas the result of local VEGF blockade is shown in the bottom series on the right. Scale bar (panels moving from right to left): 1 mm, 200 μm, 1 mm, 200 μm. Representative of four replicates.

(C) FACS plot analysis of the constituent cells of the induced cartilage (top horizontal panel) (experimental scheme as shown in Figure 7A) versus those of freshly isolated cells from ear cartilage of age-matched mice (bottom horizontal panel) demonstrates that PCPs are found in similar frequency in the induced and natural cartilage tissue. Representative of the assay performed in triplicate.

with alexa-dye-conjugated antibodies, washed, and imaged with an inverted microscope.

Cell Culture

Skeletal progenitors were cultured in MEMα medium with 10% FCS, 1% penicillin-streptomycin under low O_2 (2% atmospheric oxygen, 7.5%CO_2) conditions. For mSSC colony-forming assays, single cells were sorted into each well of a 96-well plate and cultured for 2 weeks.

Parabiosis

Age- and sex-matched congenic GFP and non-GFP mice were sutured together along the dorsal-dorsal and ventral-ventral folds of the skin flaps. Two weeks later, blood chimerism was assessed by FACS.

In Vivo Osteo-induction with BMP2

rhBMP2 was resuspended in sterile filtered buffer and applied to a collagen sponge. Sponge was lyophilized and transplanted subcutaneously into anesthetized mice.

Inhibition of VEGF Signaling

To study systemic inhibition of VEGF signaling, 10^9 pfu units of adenoviral vectors encoding the soluble murine VEGFR1 ectodomain (Ad sVEGFR1) was injected intravenously to the designated recipient mice 24 hr prior to transplantation, leading to hepatic infection and secretion of this potent antagonist of VEGF signaling into the circulation. For negative control, adenovirus encoding a murine IgG2α Fc immunoglobulin fragment was used (Ad Fc). These reagents are described elsewhere (Wei et al., 2013).

Local VEGF inhibition: 50 μg of soluble VEGFR1 was lyophilized together with recombinant BMP2 in a collagen sponge, which was then inserted into subcutaneous fat.

Single-Cell RNA Sequencing

This was performed as previously described (Treutlein et al., 2014).

Mouse Femoral Fracture ± Hindlimb Irradiation

An incision was made from the groin crease to the knee of the right femur. A medullary rod was placed via the intercondylar fossa. A bicortical transverse mid-diaphyseal fracture was created, and the skin incision closed with nylon sutures, and the mice received post-operative analgesia. The callus was harvested, and constituent cells isolated by mechanical and enzymatic dissociation and subsequent FACS fractionation. C57BL6 hindlimbs received a single dose of 800 rads (8Gy) to bilateral hind limbs. Surgical placement of fracture was performed 12 hr post-irradiation.

ACCESSION NUMBERS

The NIH GEO accession number for the microarray data reported in this paper is GSE64447. Normalized data can also be accessed through Gene Expression Commons, "Public Bone Progenitors Model."

SUPPLEMENTAL INFORMATION

Supplemental Information includes Extended Experimental Procedures and six supplemental figures and can be found with this article online at http://dx.doi.org/10.1016/j.cell.2014.12.002.

AUTHOR CONTRIBUTIONS

C.K.F.C., I.L.W., and M.T.L. conceived the overall project strategy; C.K.F.C., E.Y.S., J.Y.C., D.L., A.M., R.T., J.V.-T., T.W., W.-J.L., K.S.-Y., M.T.C., O.M., M.T., R.U., G.G.W., and A.S.L. designed, performed, and interpreted data, contributed to the writing and editing of manuscript, and prepared figures. R.S., E.Y.S., and D.S. performed single-cell RNA-sequencing/analysis; J.S. provided new algorithms for transcriptional analysis. C.K. and K.S.Y. designed and contributed reagents for vascular signaling manipulation. I.L.W. and M.T.L. edited the manuscript and supervised the laboratory.

ACKNOWLEDGMENTS

We would like to acknowledge Seth Karten for his critical help in editing the manuscript; Christopher Duldulao and Tejaswitha Naik for technical assistance; Shirley Kantoff, Libuse Jerabek, and Terry Storm for laboratory management; Aaron McCarty, Joel Dollaga, and Felix Manuel for animal care; Patty Lovelace and Jennifer Ho in the Shared FACS Facility in the Lokey Stem Cell Institute; Steve Quake, Norma Neff, Sopheak Sim, and Gary Mantalas for critical help while performing single-cell RNA sequencing; and Natalia Kosovilka and Michael Eckart at Stanford PAN Facility for help with microarray analysis. The authors would like to acknowledge ongoing support for this work: Virginia and D.K. Ludwig Fund for Cancer Research, National Institutes of Health (NIH) Grants U01HL099999, R01 CA86065, and R01 HL058770 (to I.L.W.); R01 DE021683, R21 DE024230, R01 DE019434, RC2 DE020771, U01 HL099776, and R21 DE019274 (to M.T.L.); and 1R01CA158528, 1R01NS064517, and 2U01DK085527-06 (to C.J.K.); Siebel Fellowship from Thomas and Stacey Siebel Foundation and Prostate Cancer Foundation Young Investigator Award (to C.K.F.C.); CIRM TR1-01249, the Oak Foundation, the Hagey Laboratory for Pediatric Regenerative Medicine, the Gunn/Olivier Research Fund, Stinehart-Reed Fund (to M.T.L.); the Stanford Medical Scientist Training Program, NIH-T32GM007365 (to J.Y.C.); Stanford University Transplant and Tissue Engineering Center of Excellence Fellowship (to A.M. and R.T.); the Plastic Surgery Foundation/Plastic Surgery Research Council Pilot Grant and the American Society of Maxillofacial Surgeons Research Grant (to R.T.); Burroughs Wellcome Career Award for Medical Scientists, K08 DK096048 01(to K.S.Y.); Stanford Developmental Cancer Research Award (to D.S.); the Stanford Medical Scientist Training Program, NIGMS training grant GM07365 (to G.G.W.); and the Anonymous Donor Skeletal Stem Cell Research Fund (to E.Y.S., C.K.F.C., and M.T.L.). The content is solely the responsibility of the authors and does not necessarily represent the official views of the NIH.

Received: May 26, 2014
Revised: September 22, 2014
Accepted: November 25, 2014
Published: January 15, 2015

REFERENCES

Arai, F., Hirao, A., Ohmura, M., Sato, H., Matsuoka, S., Takubo, K., Ito, K., Koh, G.Y., and Suda, T. (2004). Tie2/angiopoietin-1 signaling regulates hematopoietic stem cell quiescence in the bone marrow niche. Cell *118*, 149–161.

Bhumiratana, S., Eton, R.E., Oungoulian, S.R., Wan, L.Q., Ateshian, G.A., and Vunjak-Novakovic, G. (2014). Large, stratified, and mechanically functional human cartilage grown in vitro by mesenchymal condensation. Proc. Natl. Acad. Sci. USA *111*, 6940–6945.

Bianco, P. (2011). Bone and the hematopoietic niche: a tale of two stem cells. Blood *117*, 5281–5288.

Bianco, P. (2014). "Mesenchymal" stem cells. Annu. Rev. Cell Dev. Biol. *30*, 677–704.

Burr, D.B. (2004). The importance of subchondral bone in the progression of osteoarthritis. J. Rheumatol. Suppl. *70*, 77–80.

Calvi, L.M., Adams, G.B., Weibrecht, K.W., Weber, J.M., Olson, D.P., Knight, M.C., Martin, R.P., Schipani, E., Divieti, P., Bringhurst, F.R., et al. (2003). Osteoblastic cells regulate the haematopoietic stem cell niche. Nature *425*, 841–846.

Carlevaro, M.F., Cermelli, S., Cancedda, R., and Descalzi Cancedda, F. (2000). Vascular endothelial growth factor (VEGF) in cartilage neovascularization and chondrocyte differentiation: auto-paracrine role during endochondral bone formation. J. Cell Sci. *113*, 59–69.

Conboy, M.J., Conboy, I.M., and Rando, T.A. (2013). Heterochronic parabiosis: historical perspective and methodological considerations for studies of aging and longevity. Aging Cell *12*, 525–530.

Chan, C.K., Lindau, P., Jiang, W., Chen, J.Y., Zhang, L.F., Chen, C.C., Seita, J., Sahoo, D., Kim, J.B., Lee, A., et al. (2013). Clonal precursor of bone, cartilage,

and hematopoietic niche stromal cells. Proc. Natl. Acad. Sci. USA *110*, 12643–12648.

De Palma, M., Venneri, M.A., Galli, R., Sergi Sergi, L., Politi, L.S., Sampaolesi, M., and Naldini, L. (2005). Tie2 identifies a hematopoietic lineage of proangiogenic monocytes required for tumor vessel formation and a mesenchymal population of pericyte progenitors. Cancer Cell *8*, 211–226.

Friedenstein, A.J., Chailakhyan, R.K., and Gerasimov, U.V. (1987). Bone marrow osteogenic stem cells: in vitro cultivation and transplantation in diffusion chambers. Cell Tissue Kinet. *20*, 263–272.

Galloway, J.L., Delgado, I., Ros, M.A., and Tabin, C.J. (2009). A reevaluation of X-irradiation-induced phocomelia and proximodistal limb patterning. Nature *460*, 400–404.

Gerber, H.P., Vu, T.H., Ryan, A.M., Kowalski, J., Werb, Z., and Ferrara, N. (1999). VEGF couples hypertrophic cartilage remodeling, ossification and angiogenesis during endochondral bone formation. Nat. Med. *5*, 623–628.

Harper, J., and Klagsbrun, M. (1999). Cartilage to bone—angiogenesis leads the way. Nat. Med. *5*, 617–618.

Heldin, C.H., and Westermark, B. (1999). Mechanism of action and in vivo role of platelet-derived growth factor. Physiol. Rev. *79*, 1283–1316.

Jo, C.H., Lee, Y.G., Shin, W.H., Kim, H., Chai, J.W., Jeong, E.C., Kim, J.E., Shim, H., Shin, J.S., Shin, I.S., et al. (2014). Intra-articular injection of mesenchymal stem cells for the treatment of osteoarthritis of the knee: a proof-of-concept clinical trial. Stem Cells *32*, 1254–1266.

Kilic, G., Kilic, E., Akgul, O., and Ozgocmen, S. (2014). Decreased femoral cartilage thickness in patients with systemic sclerosis. Am. J. Med. Sci. *347*, 382–386.

Makris, E.A., Gomoll, A.H., Malizos, K.N., Hu, J.C., and Athanasiou, K.A. (2014). Repair and tissue engineering techniques for articular cartilage. Nat. Rev. Rheumatology. Published online September 23, 2014. http://dx.doi.org/10.1038/nrrheum.2014.157.

Méndez-Ferrer, S., Michurina, T.V., Ferraro, F., Mazloom, A.R., Macarthur, B.D., Lira, S.A., Scadden, D.T., Ma'ayan, A., Enikolopov, G.N., and Frenette, P.S. (2010). Mesenchymal and haematopoietic stem cells form a unique bone marrow niche. Nature *466*, 829–834.

Mitchell, M.J., and Logan, P.M. (1998). Radiation-induced changes in bone. Radiographics *18*, 1125–1136, quiz 1242–1243.

Mollon, B., Kandel, R., Chahal, J., and Theodoropoulos, J. (2013). The clinical status of cartilage tissue regeneration in humans. Osteoarthritis and cartilage / OARS. Osteoarthritis Research Society *21*, 1824–1833.

Morrison, J.I., Lööf, S., He, P., and Simon, A. (2006). Salamander limb regeneration involves the activation of a multipotent skeletal muscle satellite cell population. J. Cell Biol. *172*, 433–440.

Park, D., Spencer, J.A., Koh, B.I., Kobayashi, T., Fujisaki, J., Clemens, T.L., Lin, C.P., Kronenberg, H.M., and Scadden, D.T. (2012). Endogenous bone marrow MSCs are dynamic, fate-restricted participants in bone maintenance and regeneration. Cell Stem Cell *10*, 259–272.

Rinkevich, Y., Lindau, P., Ueno, H., Longaker, M.T., and Weissman, I.L. (2011). Germ-layer and lineage-restricted stem/progenitors regenerate the mouse digit tip. Nature *476*, 409–413.

Saito, T., Fukai, A., Mabuchi, A., Ikeda, T., Yano, F., Ohba, S., Nishida, N., Akune, T., Yoshimura, N., Nakagawa, T., et al. (2010). Transcriptional regulation of endochondral ossification by HIF-2alpha during skeletal growth and osteoarthritis development. Nat. Med. *16*, 678–686.

Seita, J., Sahoo, D., Rossi, D.J., Bhattacharya, D., Serwold, T., Inlay, M.A., Ehrlich, L.I., Fathman, J.W., Dill, D.L., and Weissman, I.L. (2012). Gene Expression Commons: an open platform for absolute gene expression profiling. PLoS ONE *7*, e40321.

Street, J., Bao, M., deGuzman, L., Bunting, S., Peale, F.V., Jr., Ferrara, N., Steinmetz, H., Hoeffel, J., Cleland, J.L., Daugherty, A., et al. (2002). Vascular endothelial growth factor stimulates bone repair by promoting angiogenesis and bone turnover. Proc. Natl. Acad. Sci. USA *99*, 9656–9661.

Treutlein, B., Brownfield, D.G., Wu, A.R., Neff, N.F., Mantalas, G.L., Espinoza, F.H., Desai, T.J., Krasnow, M.A., and Quake, S.R. (2014). Reconstructing lineage hierarchies of the distal lung epithelium using single-cell RNA-seq. Nature *509*, 371–375.

Ueno, H., and Weissman, I.L. (2006). Clonal analysis of mouse development reveals a polyclonal origin for yolk sac blood islands. Dev. Cell *11*, 519–533.

Wei, K., Piecewicz, S.M., McGinnis, L.M., Taniguchi, C.M., Wiegand, S.J., Anderson, K., Chan, C.W., Mulligan, K.X., Kuo, D., Yuan, J., et al. (2013). A liver Hif-2α-Irs2 pathway sensitizes hepatic insulin signaling and is modulated by Vegf inhibition. Nat. Med. *19*, 1331–1337.

Zhou, B.O., Yue, R., Murphy, M.M., Peyer, J.G., and Morrison, S.J. (2014). Leptin-receptor-expressing mesenchymal stromal cells represent the main source of bone formed by adult bone marrow. Cell Stem Cell *15*, 154–168.